Rana, S., Reynolds, J., Ling, T., Shamsudin, M., Pu, S., Chong, H., & Pamunuwa, D. (2018). Nano-crystalline graphite for reliability improvement in MEM relay contacts. *Carbon*, *133*, 193-199. https://doi.org/10.1016/j.carbon.2018.03.011

Nano-crystalline graphite for reliability improvement in MEM relay contacts

Sunil Rana[1], Jamie D. Reynolds[2], Ting Y. Ling[2,3], Muhammed S. Shamsudin[2,3], Suan H. Pu[2,3], Harold M. H. Chong[2], Dinesh Pamunuwa[1,*]

Abstract

Micro- and Nano-electromechanical (MEM/NEM) relays can operate with zero-leakage at far higher temperatures and levels of radiation than transistors, but have poor reliability. This work demonstrates improvement in reliability of MEM relays using nano-crystalline graphite (NCG)-coated contact surfaces. The high stability of NCG in ambient air, along with its low surface energy, appear to make it an ideal contact material. NCG-coated relays achieved over 2.8 million fast, hot-switching cycles with a drain current of at least 5 µA and on-resistance under 17 kΩ, in ambient air. The relays also were tested in slow, hot-switching cycles designed to increase the electrical stress on the contact, and consistently achieved on-currents up to 50 µA or the imposed current limit without failure. The eventual cause of failure appeared to be mechanical stress on the NCG layer over repeated cycling causing degradation. Increasing the layer thickness is expected to further improve the contact reliability. The relays are scalable and can be used as micro- or nano-scale switches in electronic components designed for very high temperatures and levels of radiation.

1. Introduction

Micro- and Nano-electromechanical (MEM/NEM) relays have zero leakage in the off-state as well as a much steeper subthreshold slope than transistors when turning off [1]. Further, MEM/NEM relays can operate at a much higher temperature [2] and radiation levels (up to two orders of magnitude higher) [3] than transistors are capable of. Thus, MEM/NEM relays have great potential to be used as micro/nano switches to build logic circuits, despite their relatively slow switching speed. For example, replacing pass transistors in interconnection switching blocks in FPGAs where the switching speed is irrelevant can achieve major energy savings [4]. Alternately, circuits made entirely of relays can transform the capability of harsh-environment electronics where radiation hardness and high temperature operation take precedence.

The switching of a NEM relay requires the making and breaking of an electrically conductive physical contact between the source and drain terminals. The reliability of this contact poses one of the most significant challenges to the deployment of NEM relay technology. The contact (and hence the relay) tends to fail through a variety of mechanisms including increased resistance due to oxidation or wear of the conductive contact material, and microwelding or stiction leading to a permanently closed relay. A number of noble/transition metals as well as their silicides have been tested to overcome contact degradation through oxidation and/or mechanical wear (e.g. Pt [5], Ru [6], W [7], PtSi [8]). Metal and semiconductor based compounds (SiGe/TiN [9], TiN [10], WN_X [11], TiO_2 [12], RuO_2 [13], SiC [14] have been investigated to reduce stiction and/or improve wear resistance. While some of these trials have achieved $> 10^6$ cycles, the test conditions (particularly on-current limit and operational environment) across most of these studies have been unrealistic for circuit-level operation; see Table 1. Moreover, different studies using the same material seem to have produced conflicting results. For example, Parsa et al. report 10^8 cycles using Pt coated contacts [5] while de Boer et al. report deterioration in Pt contacts after 10^5 cycles [13]. Our own experiments with Au and Ti in ambient air have shown deterioration after a few tens to a few hundreds of cycles.

The optimal contact material must:

- maintain mechanical/chemical integrity with sustained low 'on'-resistance (ideally in ambient air);
- exhibit low surface energy to prevent stiction-related failure;
- have a well-characterized, repeatable synthesis process compatible with standard foundry offerings, and
- achieve a low-resistance, ohmic interface with the underlying material (if present) forming the conduction path.

Further, if deposited/grown in the form of a film, the contact material must also exhibit excellent adhesion to the substrate. Due to its inertness in an ambient environment and low surface energy, different forms of carbon

*Corresponding author
Email address: dinesh.pamunuwa@bristol.ac.uk (Dinesh Pamunuwa)
[1]Department of Electrical and Electronic Engineering, University of Bristol, Bristol BS8 1UB, UK
[2]School of Electronics and Computer Science, Univer- sity of Southampton, Southampton SO17 1BJ, UK
[3]University of Southampton Malaysia Campus, 79200, Iskandar Puteri, Johor, Malaysia

Table 1: Comparison of metals, metal silicides and metallic and semiconductor-based compounds used as relay contact materials

Work	Cycles	Material	Ambient	On-current
[5]	10^8	Pt	Dry N_2	Initial 1 µA then degrades, time history not provided
[6]	3.5×10^7	Ru	-	0.1 mA at 4 V, contact I-V characteristics not provided, difficult fabrication process
[7]	0.65×10^6	W	-	Limited to 20 nA
[8]	-	PtSi	-	-
[9]	10^{10}	SiGe / TiN	Vacuum	Initial 1 nA then degrades after $\sim 10^6$ cycles
[10]	1000	TiN	-	Limited to 1 nA
[11]	-	WN_x	-	Limited to 1 nA
[12]	10^9	TiO_2	N_2	On-current not provided. On-resistance $\sim$ 10 10 kΩ
[14]	14000	poly-SiC	Air	Long hot-switch cycles. O-current starts at $\sim$ 30 nA and subsequently drops below 1 nA.

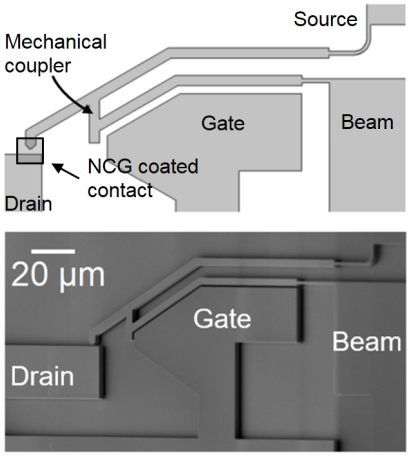

Figure 1: Relay architecture with a dual beam configuration (schematic at top and SEM micrograph at bottom). Current devices are 3-terminal devices where the source and beam terminals are connected via an electrically conductive mechanical coupler (i.e. etched out of the device silicon layer, same as the beams). Insertion of an insulating coupler will enable a single contact, 4-terminal relay.

seem to satisfy many, if not all, of these requirements.

Grogg et al. reported amorphous-carbon-coated relays that benefit from the low surface energy of carbon [15], but require a relatively high initial voltage to be applied for filament formation, and dry N_2 ambient. A few groups including Lee et al. [16], Jang et al. [17] and Loh et al. [18] demonstrated NEM relays using carbon nanotubes and diamond like carbon, but the fabrication process does not appear to be easily adaptable for large-scale fabrication. These approaches have progressed the state-of-the-art in relay contact development; however, there are still unresolved issues related to repeatability, electrical conductivity and adhesion to substrate.

This work reports on the performance of a nano-crystalline form of carbon –nano-crystalline graphite (NCG)– that greatly improves the stability and reliability of MEM relays when used as a protective coating on the relay contacts. It is deposited using a highly optimized, repeatable plasma-enhanced chemical vapour deposition (PECVD) process, where layer thicknesses of >200 nm can be readily achieved. The deposited NCG films have low surface roughness (5-8% of the film thickness) and excellent adhesion to a variety of substrates, including silicon. High on-currents (>5 µA) were consistently achieved after being stored and cycled in an environment of ambient air, showing the stability of NCG-coated relay contacts.

2. Experimental Methods and Materials

2.1. Prototype Fabrication

The relay architecture used for these experiments, shown in Fig. 1, top, consists of two parallel, cantilevered beams connected with a coupler. The relays were fabricated using silicon-on-insulator wafers with silicon device layer thickness 2 µm and resistivity 0.02 Ω-cm to 0.003 Ω-cm. The buried-oxide layer is 1 µm thick, while the handle silicon is 350 µm thick with a resistivity of 1 Ω-cm to 10 Ω-cm. A 600 nm thick SiO_2 hard mask was deposited using PECVD and patterned by a reactive ion etch (RIE). Subsequently, the device silicon layer was etched using an inductively-coupled plasma (ICP) etch step. The buried-oxide layer was then partially etched in buffered hydrofluoric (HF) acid (7:1). A 100 nm thick layer of NCG was subsequently deposited using PECVD.

The NCG was deposited by carrying out PECVD in CH_4 and H_2 plasma [19] and patterned using an oxygen-plasma RIE, such that only the beam tips and the adjacent drain regions were covered. Metal contact pads (Cr/Au) were then formed using sputtering and lift-off (for device testing). The partially suspended relays were finally fully suspended using buffered-HF-acid etch followed by critical-point drying.

2.2. NCG Friction Coefficient and Resistivity Measurement

To study the tribological properties of NCG-coated surfaces a frictional force microscopy (FFM) system - Park XE7 AFM - was used. A contact-mode AFM probe (PPP-CONTSCR, tip radius < 10 nm) was used in dry-contact

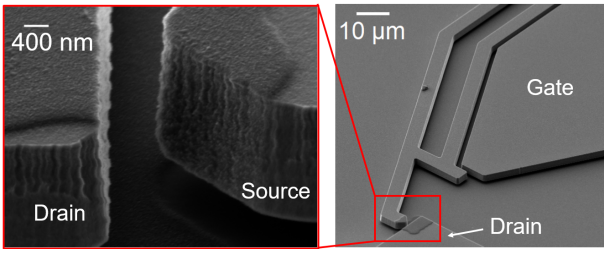

Figure 2: Relay source tip and drain coated with 100 nm thick NCG layer. The NCG layer has been lithographically patterned to cover the contact region only.

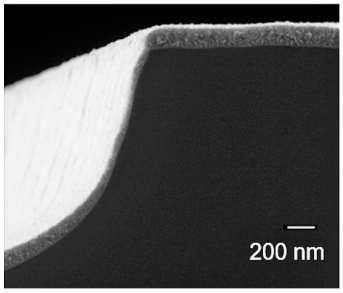

Figure 3: Helium ion microscopy image showing NCG thickness variation as a function of feature slope angle. The substrate is crystalline silicon. The layer thickness reduces for slopes close to 90, but the layer remains continuous.

lateral-force mode, in ambient air. The friction coefficients were measured at four different normal force values –1, 2, 5 and 10 nN. At each normal force value, an average of three measurements were recorded. The friction coefficients for a SiO_2-coated sample and a bare silicon sample were also measured for reference. The SiO_2 layer was thermally grown on clean Si samples in O_2 atmosphere giving a layer thickness of 280 nm. The NCG layer was deposited at 850 °C, in CH_4 and H_2 plasma for 60 min, giving a thickness of 47 nm. The corresponding average surface roughness (R_a) of all three surfaces was also recorded. The silicon sample was etched in buffered-HF acid immediately prior to measurements to remove native oxide.

In order to extract the sheet resistance of NCG, layers of varying thickness (9, 43, 85 and 195 nm) were deposited onto a 300 nm thick SiO_2 layer on a silicon wafer and measured using ellipsometry. The corresponding sheet resistance was measured using the Transmission Line Method (TLM). The TLM samples were prepared by etching the NCG layer into 240 × 1100 µm strips using RIE. A 10 nm thick Ti layer and a 400 nm thick Al layer was deposited by e-beam evaporation onto the NCG layer and lifted off into 120 × 120 µm pads for contacts. The separation length between the contact pads were 10, 15, 20, 30, 50, and 100 µm. The sheet resistance was then extracted from the average resistance measurements from 5 TLM samples against the length. This was repeated for each thickness.

2.3. Hot-switch cycling experiments

The prototype relays (effective beam length 130 µm, hinge width 2 µm, beam thickness 2 µm, simulated pull-in voltage from Ansys simulations 23 V) were first tested for their respective pull-in/out voltages (V_{pi}, V_{po}) by ramping up the gate voltage (V_g) in steps of 200 mV and monitoring the drain current (I_d). Next, the device conductance characteristics were established by applying a gate voltage $V_g > V_{pi}$ and sweeping the drain voltage (V_d) across the range −8 V to 8 V with the source grounded.

Subsequently, two types of experiments were carried out: 1) high-resolution, slow $I_d - V_g$ sweeps (i.e. "long-hot" cycling [14]) and 2) low-resolution, fast cycling. The slow $I_d - V_g$ sweeps comprised ramping of gate voltage (in steps of 200 mV) within a range larger than the relay pull-in/out hysteresis window. The on-time during each cycle was ∼ 7 s (chosen as a reasonable compromise between robustness of test and time taken to test) providing a higher average drain current than is possible with fast cycling.

In contrast, during the low resolution fast cycling experiments, the current was sampled periodically. However, in all cycles a constant drain-source bias was applied (with a compliance, i.e. limit, of 5 µA[1]), so that conduction took place. The relays were switched for 3650 cycles by applying V_g pulses at 90 Hz that switched between 25 V (on) and 5 V (off). Every 72 cycles, two I_d values were logged for on and off states, i.e. in a sequence of 3650 cycles, there were 50 cycles where I_d was recorded. After a 3650 cycle sequence, one switching cycle was carried out where V_g was incremented in steps of 25 mV, from 0 V to 25 V and back down to 0 V. These sweeps were used to monitor the change in the relay pull-in/out hysteresis window as the fast cycling progressed. An Agilent B1500A semiconductor parameter analyzer was used for the slow sweeps, while a dual channel Keithley 2602 source measure unit (SMU) was used for fast hot-switching. Both experiments were carried out in ambient air, at room temperature on a number of relays. The relays tested were fabricated in separate batches but had the same design.

3. Results and Discussion

A fabricated relay, with patterned NCG on the source tip and adjacent drain is shown in Fig. 2. Sidewall coverage is achieved, though the layer thickness varies depending on the feature angle (Fig. 3). While the layer thickness is higher on flat regions and becomes thinner with increasing sidewall angles, the layer remains continuous. This is seen on the fabricated relays as well, where the NCG layer thickness is greater on the planar regions compared to the sidewalls (Fig. 2 inset).

3.1. Characterisation of NCG

The NCG characteristics were measured using Raman spectroscopy with excitation laser wavelength of 532 nm.

[1]Relays operating as switches in digital circuits will typically have a fanout load well under 1 µA.

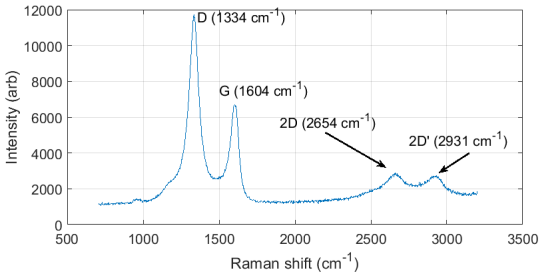

Figure 4: Raman spectra of NCG deposited on a Si substrate, over a 90 nm thick layer of SiO_2 using PECVD at 850 °C.

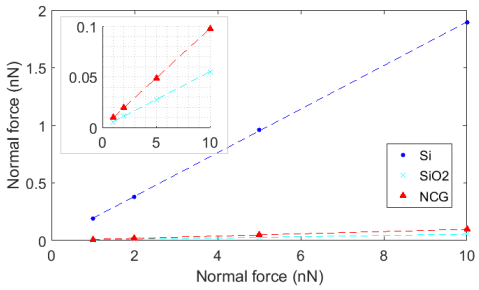

Figure 5: Friction force measurement for Si, SiO_2 on Si and NCG on Si substrates. The measured friction coefficient varies from 0.0055 for SiO_2 to 0.1892 for Si.

The Raman spectra (Fig. 4) show prominent D and G peaks which confirm the presence of sp^2 hybridized carbon atoms. The presence of the broad second-order D peak, also known as the 2D peak, indicates a thick layer having a graphitic lattice structure. The presence of the shifted 2D' peak is due to the second-order intra-valley double resonance effect in the lattice structure, which confirms the presence of grain boundary defects and NCG [20]. The surface friction and electrical properties of deposited NCG layers on various substrates are discussed in Section 3.2.

3.2. Friction coefficient and resistivity measurement

A comparison of friction coefficients measured on SiO_2, Si and NCG-coated Si substrates is shown in Fig. 5 and summarized in Table 2. The friction coefficient does not necessarily correlate with the surface roughness [21]. Despite the comparatively higher surface roughness, the friction coefficient of the NCG layer was comparable to that of SiO_2 –roughly two orders of magnitude smaller than that of Si. The sheet resistance measurements for different NCG layer thickness values are shown in Fig. 6. The slope of the sheet resistance plotted against inverse thickness is a measure of resistivity of the deposited films, and is 10.3 mΩ-cm.

3.3. $I_d - V_d$ sweeps for conductance characterisation

The drain current (I_d) dependence on drain voltage (V_d) is shown in Fig. 7. The relays consistently achieved

Table 2: A summary of the average surface roughness, and the corresponding friction coefficient, for bare, clean silicon and Si substrate coated with NCG

Material	Surface roughness average (nm)	Friction coefficient
Bare silicon	0.1505	0.18920
SiO_2	0.051	0.00550
NCG on Si	1.477	0.00976

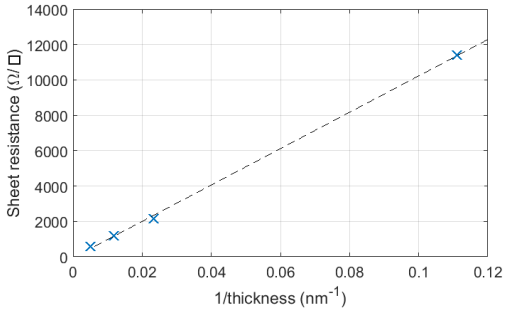

Figure 6: Variation in NCG sheet resistance with inverse of layer thickness. The extracted resistivity is 10.3 mΩ-cm

on-currents greater than 50 µA, and for very high currents (>0.5 mA), the I_d dependence on V_d appears to be mildly non-linear. The on-resistance calculated over the range −3 V to 3 V is 16.4 kΩ. Other tested relays achieved broadly similar, though not identical, conductance characteristics[1]. Since there is no rectifying behaviour, the relay conducts even at low drain voltages, a desirable characteristic in bulding efficient and low-power logic circuits. This is in contrast with amorphous-carbon contacts demonstrated by Grogg *et al.* [15] which require carbon filament formation to become conductive, at drain voltages of 1.5 V to 2.5 V.

3.4. High resolution, slow $I_d - V_g$ sweeps

The slow $I_d - V_g$ experiments comprise 750 'long hot-switching cycles', where the relays remain in the 'on', conducting state, for ∼7 s during each cycle. The total on-time (i.e. drain conducting) is ∼5250 s. The principal objective of this experiment is to place electrical stress on the relay. In the on-state, the source-drain contact region of the relay is expected to present the highest resistance to the source-drain current path. If present, Joule-heating related failure mechanisms (including microwelding), should manifest during these experiments. The slow sweep measurements are shown in Fig. 8. The current compliance limit is set at 1 µA, which is reached on every cycle. There is no appreciable change in the relay performance during this experiment, indicating that Joule-heating related degradation is unlikely to be a failure mechanism.

[1]Residual stress causes the beam to bend slightly out of plane on release, resulting in the contact area being slightly different for different devices.

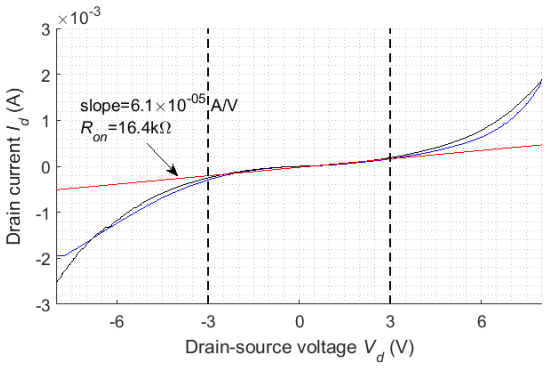

Figure 7: Slow $I_d - V_d$ sweep showing conductance characteristic for 43 nm thick layer. The relays were pulled-in ($V_g = 23$ V) before the V_d sweep. The 'on' resistance in the range -3 V to 3 V is 16.4 kΩ. Over a wider range, the 'on' resistance is less. 'On' currents up to 50 µA were consistently reached. Other tested devices showed similar, though not identical characteristics.

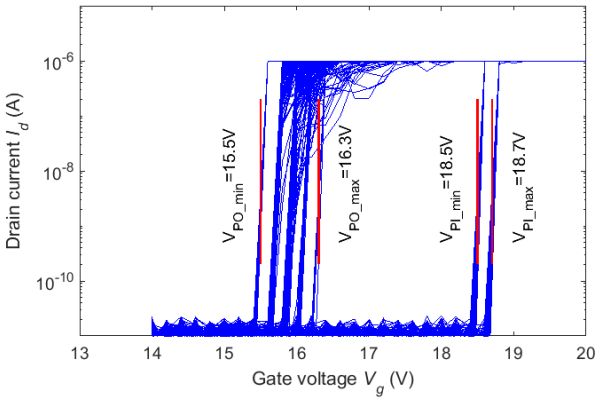

Figure 8: Slow $I_d - V_g$ sweep showing conduction for 750 cycles (relay 1). A drain current compliance limit of 1 µA was imposed, which was hit every time. The periodic variation in the pull-in/out traces corresponds to the 200 mV step size of the V_g sweep. V_d was kept at 1 V.

3.5. Low resolution fast cycling with high resolution $I_d - V_g$ sweeps

The low resolution fast cycling (or short hot-switching) experiment is carried out to place mechanical stress on the relays especially on the source-drain contact region. Most relays seemingly fail due to degradation of the contact surfaces. The fast cycling experiments should reveal failure mechanisms related to mechanical wear of the contact surfaces. Other contact failure mechanisms, such as surface oxidation or contamination, are considered exclusive of mechanical wear, which can also occur during storage.

These cycling measurements are shown in Fig. 9. The current compliance limit of 5 µA is reached for over 2.8 million cycles with brief reductions in the on-current around 1.6 million and 2.05 million cycle marks. After 2.8 million cycles (an on-time of >63 650 s) the relay continued to cycle with a reduced on-current, and did not suffer mechanical failure. Cycling was halted after ∼3.62 million cycles. Other relays from the same fabrication batch that were tested achieved a similar number of fast hot-switch cycles, and a similar recovery phase was also observed after a small drop in on-current, for varying lengths of time.

Interspersed amongst the low resolution fast switching cycles are high-resolution $I_d - V_g$ sweeps where V_g is swept in increments of 0.25 V and I_d is recorded at every point. These sweeps provide important insight into the change in the relay pull-in/out behaviour, with increasing switching cycles, which would otherwise not be observed with the low-resolution, fast switching. The $I_d - V_g$ sweeps are collated in eight groups referred to as segments (Fig. 10). The eight segments in total comprise a duration of ∼2.92 million cycles (∼66 400 s), and the segments are of equal time spans.

3.6. Contact degradation

As the experimental set-ups for the slow $I_d - V_g$ sweeps and the fast cycling experiments remained constant, it is assumed that any change in the on-current is due to contact degradation. The relay behaviour did not change appreciably during the slow $I_d - V_g$ sweeps, indicating that Joule-heating related failure mechanisms may not be present. The on-current did change during the fast cycling experiments (Fig. 9), indicating that the source-drain contact evolves with repeated cycling. The momentary drop and recovery in drain current suggests a possible shift in the NCG layer at the contact. The crucial evidence comes from the $I_d - V_g$ sweeps conducted at regular intervals during fast cycling. During the first half of the experiment (Fig. 10a –10e) the pull-out systematically decreases and the hysteresis window widens. This trend can clearly be seen in Fig. 10i which plots the *average* pull-out, i.e. the mean across all pull-out values in a segment, to avoid the effect of skewing by outliers.

The width of the pull-in/out hysteresis window is a function of device geometry and the surface forces acting between the contact surfaces [22]. Since the geometrical parameters remain unchanged during the experiments, the contact surface forces seem to be responsible for the hysteresis window widening. Environmental contamination, particularly the formation of liquid thin films (leading to capillary forces), can increase surface forces; however, this explanation is discounted because such film formation can also happen during storage (the devices were stored in an ambient environment). Therefore, the most plausible explanation is the wear of the NCG layer at the contact surfaces leading to an increase in surface forces. This also explains the decrease in on-current during the fast cycling experiments. Post cycling images show degradation of the NCG layer (see supplementary material), offering corroboration of this hypothesis.

Towards the end of segment 5 (∼1.6 million cycles) the

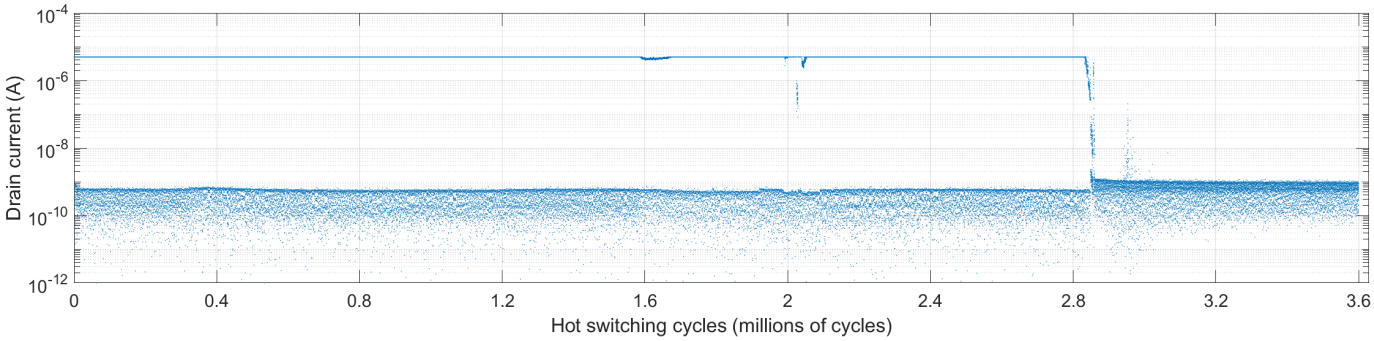

Figure 9: Low resolution, fast cycling results showing on-state and off-state drain current for each cycle. The drain voltage was kept at 1 V. and a drain current compliance limit of 5 µA was set. The drain current limit was met for over 2.8 million cycles, with a brief blip at around 2.05 million cycles. After ∼2.8 million cycles, the relay continued to cycle mechanically without failure, but did not meet the drain current compliance.

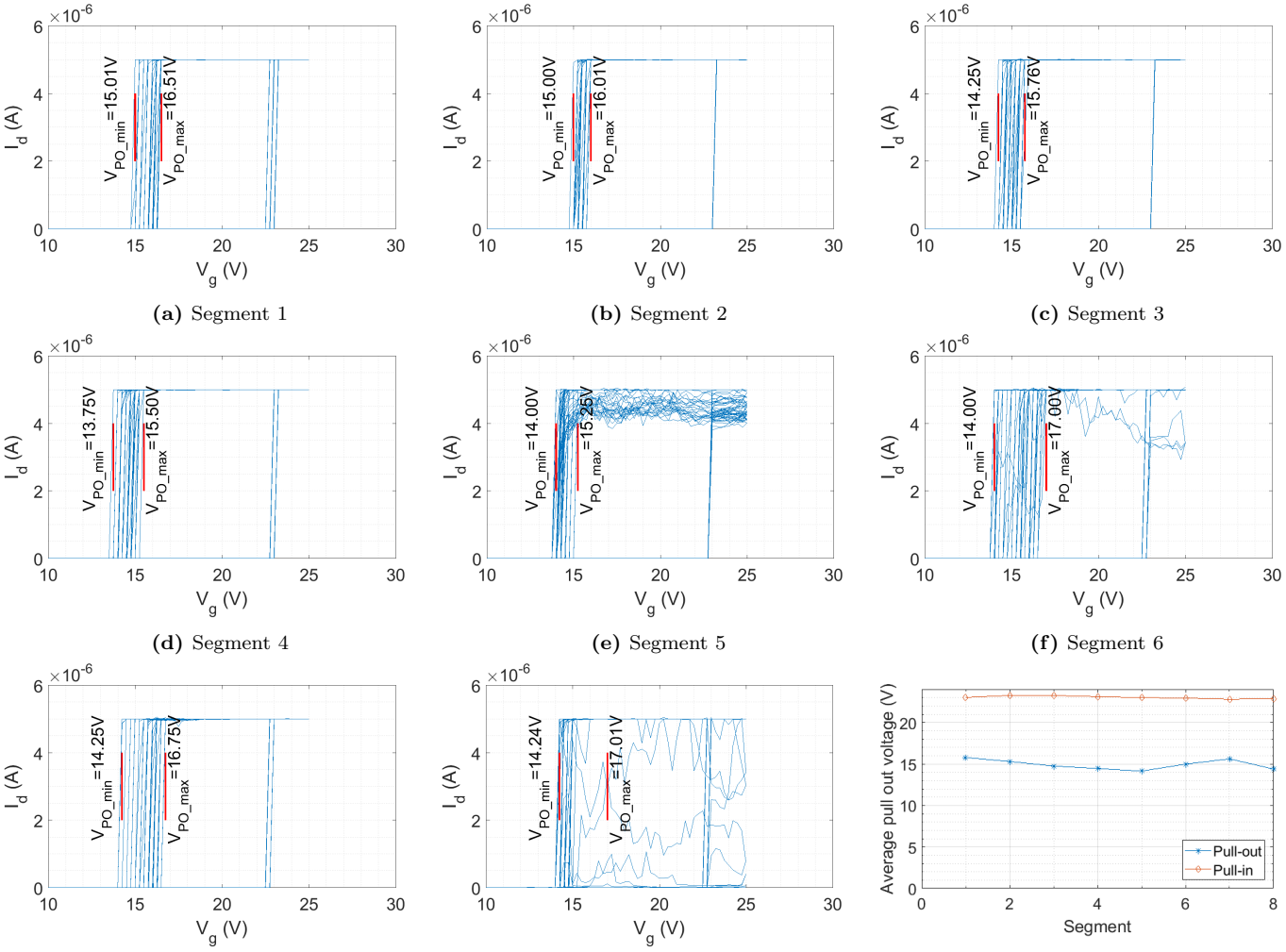

(a) Segment 1 **(b)** Segment 2 **(c)** Segment 3

(d) Segment 4 **(e)** Segment 5 **(f)** Segment 6

(g) Segment 7 **(h)** Segment 8 **(i)** Variation of pull-out and pull-in voltage.

Figure 10: Fast (high-resolution) sweep cycles were interspersed within the low-resolution fast cycles at regular intervals (after every 3650 cycles). These are shown in (a) through (h). The pull-out voltage consistently reduces until ∼1.6 million cycles (e), when the drain current starts to drop. The widening of the hysteresis window over this period suggests an increase in surface-interaction forces at the source tip-drain interface. Then it recovers before undergoing a second current-reduction and -recovery phase (f and g). In segment h, the electrical contact deteriorates again, coinciding with the pull-out reducing. For the noisy data in (h) the threshold for pull-in (out) was set as the drain current increasing (decreasing) beyond 2.5 µA, the mid-point of the compliance. The gate voltage was changed in steps of 0.25 V, accounting for the deviation from the vertical seen on the graph. In reality, the slope is as near vertical as is possible to discern based on the limitations of the measuring equipment. The variation of the average pull-out voltage is shown in (i).

contact resistance starts to increase, as can be seen in Fig. 10e. The drain current then recovers, coinciding with the hysteresis window narrowing, suggesting a redistribution of NCG resulting in reduced surface forces. Following another short blip (Fig. 10f) and recovery phase (Fig. 10g), the pull-out reduces again (Fig. 10h), indicating degradation of the NCG layer. It appears that the impact stress over repeated cycling causes displacement of NCG, eventually thinning enough that the resistance increases significantly. The relays continued to cycle mechanically with near constant pull-in, until the experiments were halted. As can be seen in Fig. 2 the NCG layer thickness on the sidewalls is comparatively thin. Thus, it appears a thicker layer can be an effective solution to further improve the electrical integrity of the relay over its life-cycle.

4. Conclusions

The electrical and tribological properties of NCG were characterised to demonstrate that it is a suitable material for relay contact surface coatings. The friction coefficient of NCG layers is two orders of magnitude lower than that of silicon. Thus, it is an appealing anti-stiction coating material for relay contacts (as well as other MEMS applications). A layer of NCG deposited directly on highly doped n-type silicon (resistivity: 0.02 Ω-cm to 0.003 Ω-cm) appears to readily form an ohmic junction. This significantly simplifies the relay fabrication process by obviating the need for conductive metal or silicide layers. Thus, the residual stresses introduced by metal/silicide layers can be completely avoided. The NCG deposition process is well optimized, enabling precise control over layer thicknesses. Crucially, the storage and subsequent operational performance of relays in ambient air indicates that NCG-coated contacts are inert and stable in an ambient environment. Thus, NCG-coated relays may reduce the need for complex and expensive hermetic packaging solutions.

NCG-coated relays presented here demonstrated a stable electrical contact and maintained a current of 5 µA in sustained switching for over 2.8 million cycles. A detailed qualitative study of the NCG coated contact, however, indicates that repeated cycling gradually affects the on-resistance as well as the surface force. This is most likely due to mechanical degradation of the NCG layer on the contact surface. The characterisation of the deposited NCG layer indicates that a thicker sidewall layer should provide further improvements in contact performance and reliability. The work presented here demonstrate how monocrystalline silicon relays can be coated with NCG to realise reliable contacts, the main point of failure that has held back their deployment.

Acknowledgements

Support from Innovate UK under grant 61931-453231, and the Malaysian Ministry of Higher Education for PhD scholarship is gratefully acknowledged.

References

[1] V. Pott, H. Kam, R. Nathanael, J. Jeon, E. Alon, T. J. K. Liu, Mechanical computing redux: Relays for integrated circuit applications, Proceedings of the IEEE 98 (12) (2010) 2076–2094. doi:10.1109/JPROC.2010.2063411.

[2] T.-H. Lee, S. Bhunia, M. Mehregany, Electromechanical computing at 500 C with silicon carbide, Science 329 (5997) (2010) 1316–1318.

[3] H. R. Shea, Effects of radiation on MEMS, in: Proc. SPIE MOEMS-MEMS, 2011, pp. 79280E–79280E.

[4] C. Chen, R. Parsa, N. Patil, S. Chong, K. Akarvardar, J. Provine, D. Lewis, J. Watt, R. T. Howe, H.-S. P. Wong, S. Mitra, Efficient FPGAs using nanoelectromechanical relays, in: Proc. ACM/SIGDA Int. Symp. Field Programmable Gate Arrays, FPGA '10, ACM, New York, NY, USA, 2010, pp. 273–282. doi:10.1145/1723112.1723158.
URL http://doi.acm.org/10.1145/1723112.1723158

[5] R. Parsa, W. S. Lee, M. Shavezipur, J. Provine, R. Maboudian, S. Mitra, H. S. P. Wong, R. T. Howe, Laterally actuated platinum-coated polysilicon NEM relays, Journal of Microelectromechanical Systems 22 (3) (2013) 768–778. doi:10.1109/JMEMS.2013.2244779.

[6] I. R. Chen, Y. Chen, L. Hutin, V. Pott, R. Nathanael, T. J. K. Liu, Stable ruthenium-contact relay technology for low-power logic, in: Int. Conf. Solid-State Sensors, Actuators and Microsystems, 2013, pp. 896–899. doi:10.1109/Transducers.2013.6626912.

[7] B. Davidson, D. Seghete, S. George, V. Bright, ALD tungsten NEMS switches and tunneling devices, Sensors and Actuators A: Physical 166 (2) (2011) 269 – 276. doi:https://doi.org/10.1016/j.sna.2009.07.022.
URL http://www.sciencedirect.com/science/article/pii/S0924424709003446

[8] D. Grogg, U. Drechsler, A. Knoll, U. Duerig, Y. Pu, C. Hagleitner, M. Despont, Curved in-plane electromechanical relay for low power logic applications, Journal of Micromechanics and Microengineering 23 (2) (2013) 025024.
URL http://stacks.iop.org/0960-1317/23/i=2/a=025024

[9] M. Ramezani, S. Severi, A. Moussa, H. Osman, H. A. C. Tilmans, K. D. Meyer, Contact reliability improvement of a poly-sige based nano-relay with titanium nitride coating, in: Int. Conf. Solid-State Sensors, Actuators and Microsystems, 2015, pp. 576–579. doi:10.1109/TRANSDUCERS.2015.7180989.

[10] D. Lee, W. S. Lee, J. Provine, J. O. Lee, J. B. Yoon, R. T. Howe, S. Mitra, H. S. P. Wong, Titanium nitride sidewall stringer process for lateral nanoelectromechanical relays, in: Int. Conf. Micro Electro Mechanical Systems (MEMS), 2010, pp. 456–459.

[11] A. M. Mayet, A. M. Hussain, M. M. Hussain, Three-terminal nanoelectromechanical switch based on tungsten nitridean amorphous metallic material, Nanotechnology 27 (3) (2015) 035202.

[12] H. Kam, V. Pott, R. Nathanael, J. Jeon, E. Alon, T.-J. K. Liu, Design and reliability of a micro-relay technology for zero-standby-power digital logic applications, in: IEEE Int. Electron Devices Meeting (IEDM), 2009, pp. 1–4.

[13] M. P. de Boer, D. A. Czaplewski, M. S. Baker, S. L. Wolfley, J. A. Ohlhausen, Design, fabrication, performance and reliability of Pt- and RuO2 -coated microrelays tested in ultra-high purity gas environments, Journal of Micromechanics and Microengineering 22 (10) (2012) 105027.
URL http://stacks.iop.org/0960-1317/22/i=10/a=105027

[14] T. He, R. Yang, S. Rajgopal, M. A. Tupta, S. Bhunia, M. Mehregany, P. X. L. Feng, Robust silicon carbide (SiC) nanoelectromechanical switches with long cycles in ambient and high temperature conditions, in: Int. Conf. Micro Electro Mechanical Systems (MEMS), 2013, pp. 516–519. doi:10.1109/MEMSYS.2013.6474292.

[15] D. Grogg, C. L. Ayala, U. Drechsler, A. Sebastian, W. W. Koelmans, S. J. Bleiker, M. Fernandez-Bolanos, C. Hagleitner, M. Despont, U. T. Duerig, Amorphous carbon active contact

layer for reliable nanoelectromechanical switches, in: Proc. Int. Conf. Micro Electro Mechanical Systems (MEMS), 2014, pp. 143–146.

[16] S. W. Lee, D. S. Lee, R. E. Morjan, S. H. Jhang, M. Sveningsson, O. A. Nerushev, Y. W. Park, E. E. B. Campbell, A three-terminal carbon nanorelay, Nano Letters 4 (10) (2004) 2027–2030. doi:10.1021/nl049053v.
URL https://doi.org/10.1021/nl049053v

[17] J. Jang, S. Cha, Y. Choi, G. A. Amaratunga, D. Kang, D. Hasko, J. Jung, J. Kim, Nanoelectromechanical switches with vertically aligned carbon nanotubes, Applied Physics Letters 87 (16) (2005) 163114.

[18] O. Loh, X. Wei, J. Sullivan, L. E. Ocola, R. Divan, H. D. Espinosa, Carbon-carbon contacts for robust nanoelectromechanical switches, Advanced Materials 24 (18) (2012) 2463–2468.

[19] M. E. Schmidt, C. Xu, M. Cooke, H. Mizuta, H. M. H. Chong, Metal-free plasma-enhanced chemical vapor deposition of large area nanocrystalline graphene, Materials Research Express 1 (2) (2014) 025031.
URL http://stacks.iop.org/2053-1591/1/i=2/a=025031

[20] A. C. Ferrari, Raman spectroscopy of graphene and graphite: Disorder,electronphonon coupling, doping and nonadiabatic effects, Solid State Communications 143 (1) (2007) 47 – 57, exploring graphene. doi:https://doi.org/10.1016/j.ssc.2007.03.052.

[21] B. N. Persson, Sliding friction: physical principles and applications, Springer Science & Business Media, 2013.

[22] K. Akarvardar, C. Eggimann, D. Tsamados, Y. Chauhan, G. Wan, A. Ionescu, R. Howe, H. P. Wong, Analytical modeling of the suspended-gate FET and design insights for low-power logic, IEEE Transactions on Electron Devices 55 (1) (2008) 48–59. doi:10.1109/TED.2007.911070.